# INVESTIGATION OF NUMERICAL SCHEMES IN AIR CAVITY COMPUTATIONS

S. Menon*, R. Bensow and C. Eskilsson
Department of Shipping and Marine Technology, Chalmers University of Technology
SE 41296, Sweden
*menon@chalmers.se

**ABSTRACT:** Air cavity and air chamber concepts have been proven to be an efficient way for drag reduction in low-speed ships. Series of experiments were conducted in the SSPA cavitation tunnel to simulate the working conditions of an air filled cavity under the hull of a ship. In this paper, study is extended with a numerical validation using a CFD Open Source solver, OpenFOAM ® (OF). Volume of fluid (VOF) approach, which uses phase volume fraction ($\alpha$) is used to compute the incompressible two-phase viscous flow. The influence of different numerical methodologies on the advection of $\alpha$ is studied. Different schemes from diffusive first-order to higher order TVD (Total Variation Dimensioning) schemes like SUPERBEE are tested. Results are also drawn from counter-gradient convective flux implementation in OF VOF approch. Conclusions are drawn from the wave profile, wave sloshing pressure force and viscous force. It was observed that, as more compressive interface capturing methods were used, the aft force was better predicted but distorts the wave profile and under predicts the beach plate force.

## 1. INTRODUCTION

A promising drag reduction technique is based on air induced lubrication under the hull of the ship. Various air induced lubrication techniques have been researched in the past [1], [2], [3], [4] and [5]. There are different techniques for the same; one of the most effective ones is where air is injected into a specifically profiled cavity or recess located under the hull. A steady air layer formed inside this cavity curtails the wetted surface and consequently reducing the skin-friction drag of the hull.

Various studies have been carried out by SSPA in collaboration with Stena Teknik and Chalmers (Sweden), on the hull and cavity profiles, starting out with Stena P-MaxAir and later Stena AirMax with 1:12 model scale. To simplify the test case for the accurate experimental measurement and testing, a simplified hull cavity profile was constructed inside a rectangular cavitation tunnel. Series of experimental testing, [6], were carried was out in the SSPA cavitation tunnel on this simplified cavity profile. The experiments mimicked the working condition of the air cavity under the hull, under steady flow conditions. Details of the geometry are given in section 1.1. Predominately, research in this field has been confined to experiments. In this paper, research accentuate computational analysis of the experiments conducted.

### 1.1 Geometry

Fig. 1a shows the three dimensional geometry on which computational study was conducted to replicate the experiments. In experiments, width of the tunnel is extended further than the width of the cavity to nullify the side wall effects. The rectangular water channel is 9.6m in length, 1m in width and 1.5m in height. An air filled cavity of 6m length and 0.1m height lies on top of this channel. The cavity has backward-facing step at the upstream end and gentle forward recline at the downstream end, which forms the closure of the cavity. The cavity roof have a length of 5.7m after which the beach plate starts. The beach plate have an acute angle

of 18.43° (with respect to the flow direction) or a length ratio of opposite side to adjacent side as 1:3. the air inlet has height of the 0.08m and 1m width. Fig. 1b, shows the schematic two dimensional model of air cavity ship. Here, $P_c$ is cavity pressure and $P_0$ is pressure at the corner of the backward-facing step. $P_0$ is taken as zero for this study and pressure at the air-inlet is specified relation to $P_0$.

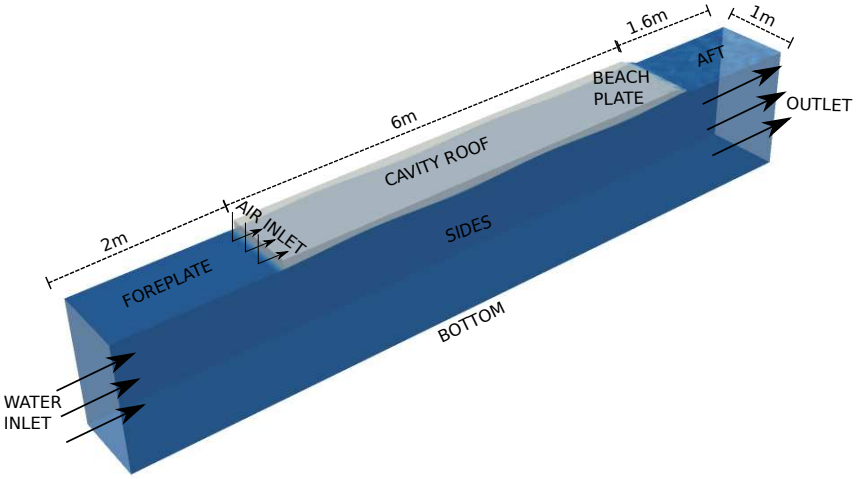


(a)

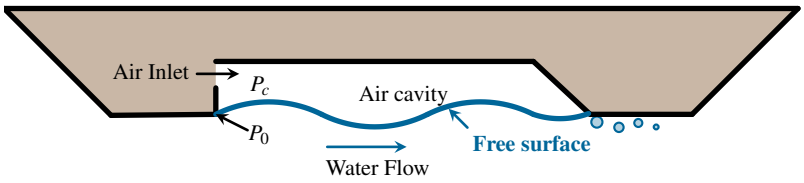


(b)

**Figure 1**: (a) The 3D geometry for air cavity test case. (b) A schematic model of the air-cavity profile. The direction of the flow of water and air is from left to right as illustrated by the arrows.

## 2. NUMERICAL FORMULATION

### 2.1 Governing equations

The governing equation for isothermal and incompressible, immiscible fluids include the continuity and momentum equations given as,

$$\frac{\partial v_i}{\partial x_i} = 0 \tag{1}$$

$$\frac{\partial v_i}{\partial t} + \frac{\partial v_i v_j}{\partial x_j} = -\frac{1}{\rho}\frac{\partial p}{\partial x_j} + \nu \frac{\partial^2 v_i}{\partial x_j \partial x_j} + g_i + \mathbf{F}_\sigma$$

where, $\mathbf{F}_\sigma$ is the volumetric surface tension force, $g_i$ is the gravitational acceleration, $\rho$ is the material density and $p$ is the pressure.

### 2.2 Volume of Fluid

The Volume of Fluid (VOF) method [7], is defined with scalar variable, $\alpha$, to distinguish two liquids with different material properties in a computational domain. The interface is smeared

over the cells where $\alpha \in [0,1]$. At the interface, computation of viscosity, density and surface tension vary according to computation of this $\alpha$ variable.

The advection equation of $\alpha$ is given as,

$$\frac{\partial \alpha}{\partial t} + \frac{\partial \alpha v_j}{\partial x_j} - \alpha \frac{\partial v_j}{\partial x_j} = 0, \tag{2}$$

For large density ratios, the main challenge for advecting the $\alpha$ variable is to preserve the mass conservativeness while guaranteeing boundedness. OpenFOAM uses an algebraic approach based on the counter-gradient transport to advect the volume fraction $\alpha$, [8]. This scheme adds a compressive term to the $\alpha$ advection equation in order to retain the conservativeness, convergence, and boundedness [9], which reduces to zero as the mesh is refined. This advective equation can be written as,

$$\frac{\partial \alpha}{\partial t} + \frac{\partial \alpha v_j}{\partial x_j} + \frac{\partial v_j^c \alpha(1-\alpha)}{\partial x_j} = 0. \tag{3}$$

where $v^c$ ensures compression ($v^c = v^l - v^g$, $l$ and $g$ stands for liquid and gas, respectively), while the $\partial/\partial x_j$ guarantees conservation and $\alpha(1-\alpha)$ guarantees boundedness. Additionally, compressive factor $c\alpha$ is used to increase compression as,

$$v^c = \min(c\alpha|v|, \min|v|)\frac{\nabla \alpha}{|\nabla \alpha|} \tag{4}$$

### 2.3 Computational setting

For computational validation, a specified experimental case [6], was chosen where in the pressure at the air inlet and water velocity are specified. The water inlet velocity is 2m/s (corresponds to 16 knots cruising speed of the real ship) and pressure at the air inlet is -100 Pa. Note that, the pressure specified ($p_{\rho gh}$) is absolute pressure minus $\rho gh$. The pressure is specified to attain an air-inlet flux of the $0.001132 m^3/s$ which corresponds to an air inlet velocity of the $0.0165 m/s$. The outlet pressure ($p_{\rho gh}$) has fixed zero value to give reference pressure and stability in the domain. Additional boundary conditions are given in table 1.

The fluid is assumed to be incompressible. Turbulence is modelled with Reynolds-averaged Navier–Stokes (RANS) equations, with $k-\omega$ SST turbulence model, and with the wall models for turbulence kinetic energy ($k$) and specific dissipation ($\omega$). The surface tension coefficient is taken as 0.0072 N/m and the surface tension is calculated by the Continuum Surface Force Model (CSF) without the density averaging proposed by Brackbill et al. [10].

Equations for velocity and pressure are solved using the Pressure Implicit with Splitting of Operators (PISO) [11]. Two pressure correction steps are used ensuring that the continuity residuals remained always below $10^{-7}$. Pressure correction equation is solved with Preconditioned Conjugate Gradient solver preconditioned with a Generalised Geometric-Algebraic Multi-grid method and Gauss-Seidel smother with two sweeps.

The $\alpha$ variable, velocity and turbulent quantities are solved with Gauss-Seidel solver. The convective term is discretised by the Gaussian integration with the limited linear or linear upwind differencing. Limited linear is the linear scheme limited to keep it bounded and linear upwind differencing (LU) involves two upstream values. Euler is used for time discretisation.

### 2.4 Interface Capturing

Many schemes to capture the non-linear convective term in the Navier-Stokes equation have been developed over the years. The boundedness while discretisation of this convection term

| Field | Water-inlet | Air-inlet | Walls | Outlet |
|---|---|---|---|---|
| prgh (Pa) | Vc | -100 | Vc | zero |
| U (m/s) | 2m/s | Pc | zero | zero gradient |
| $\alpha$ | 1 | 0 | zero gradient | zero gradient |
| $k$ $(m^2/s^2)$ | 0.015 | $1.02 \times 10^{-4}$ | wall function | zero gradient |
| $\omega$ $(s^{-1})$ | 2.13 | 0.2635 | wall function | zero gradient |

Table 1: The boundary conditions for the air cavity case. Here, prgh is $p - \rho gh$, Vc is velocity corrected pressure gradient and Pc is the pressure corrected velocity. The sides of the tunnel are given symmetric conditions.

has been a widely discussed research. OpenFOAM uses blending differencing scheme as,

$$\phi_f = (1-\gamma_f)\phi_f^{UD} + \gamma_f \phi_f^{CD} \tag{5}$$

where $\phi_f$ is the flux at the face between cell $i$ and $i+1$. $\phi_f^{UD}$ is the face flux from upwind differencing which is first order and bounded and $\phi_f^{CD}$ is the face flux from central differecing which is second order but violates boundedness. The blending factor, $\gamma_f$, is evaluated on the limiting functions.

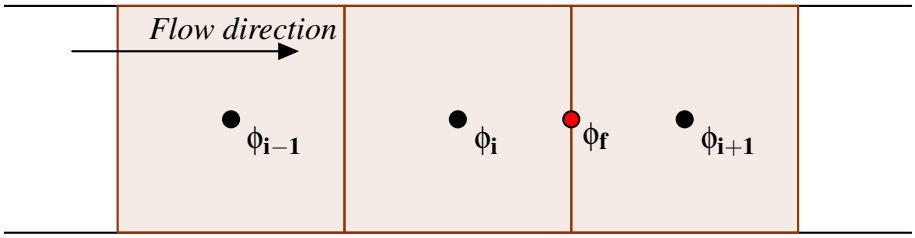


**Figure 2**: Variation of $\phi$ across the face

The families of total variation diminishing (TVD) and normalised variable diagram (NVD) differencing schemes are the well established and accepted among many others. All of these use some sort of an unboundedness indicator in order to determine the parts of the domain where intervention in the discretisation is required and limits the face value to give oscillation-free (free of overshoots and undershoots) solutions. Also, according to the TVD and NVD, any differencing scheme that is more than first-order accurate must be non-linear in order to guarantee boundedness. Non-linearity of the differencing scheme is introduced through the dependence of the flux limiter in accordance to TVD/NVD criteria. In TVD scheme, face flux is written as,

$$\phi_f = \phi_i + \frac{1}{2}\psi(r)(\phi_{i+1} + \phi_i), \tag{6}$$

where $\psi(r)$ is the limiting variable [12]. Two schemes, that are studied in this paper are given in the table 2.

### 2.4.1 CICSAM

The CICSAM (Compressive Interface Capturing Scheme for Arbitrary Meshes) scheme implemented here [15], has some changes from Ubbink [16]. The upwind cell flux is defined as,

$$\phi_{i-1}^* = \phi_{i+1} - 2(\nabla\phi_i \cdot d_f), \tag{7}$$

| Name | Limiter function $\psi(r)$ |
|---|---|
| Van Leer [13] | $\frac{r+\lvert r\rvert}{1+r}$ |
| SUPERBEE [14] | $\max[0,\min(2r,1),\min(r,2)]$ |

Table 2: Schemes used for $\alpha$ convective term. Here $r = (\phi_i - \phi_{i-1})/(\phi_{i+1} - \phi_i)$

where $d_f$ is the vector between the cell centers of the donor (cell $i$) and acceptor (cell $i+1$) cells, pointing from the donor cell towards the acceptor cell. The above approximation does not guarantee a bounded $\phi^*_{i-1}$, therefore it is necessary to bound it with known bounds of $\phi$. The bounds can be either the maximum and minimum value of the whole flow or local values derived from the cell's nearest neighbours, $\phi^{min}_{i-1} \leq \phi^*_{i-1} \leq \phi^{max}_{i-1}$. The flux at the cell is defined in the form of NVD as,

$$\tilde{\phi_i} = \frac{\phi_i - \phi^*_{i-1}}{\phi_{i+1} - \phi^*_{i-1}}. \tag{8}$$

Here it is assumed that $\mathbf{v}_f \cdot S_f > 0$.

The derivation of CICSAM is completed with the definition of weighting factor ($\gamma_f$) which is based on the cosine of the angle ($\theta_f$) between the vector normal to the interface ($\nabla\phi_i$) and the vector $d_f$. The cosine of the angle is defined as,

$$\cos\theta_f = \left| \frac{\nabla\phi_i \cdot d_f}{|\nabla\phi_i||d_f|} \right|. \tag{9}$$

There are three switching factors, $k_1, k_2$ and $k_3$ that are used to work across different Courant numbers ($Co_f$) in mesh domain. These switching factors are defined as,

$$k_1 = \frac{3Co_f^2 - 3Co_f}{2Co_f^2 + 6Co_f - 8}, \qquad k_2 = Co_f, \qquad k_3 = \frac{3Co_f + 5}{2Co_f + 6}. \tag{10}$$

Definition of weighting factor ($\gamma_f$) is given in the table 3.

### 2.4.2 Interface Compression

Interface compression scheme, [17], is based on the generic limited scheme but, it does not use the NVD/TVD functions. The scheme is used for the counter-gradient convective term in the $\alpha$ transport equation. It is defined as,

$$\gamma_f = 1 - max[(1 - 4\phi_i(1-\phi_i))^2, (1 - 4\phi_{i+1}(1-\phi_{i+1}))^2]. \tag{11}$$

### 2.4.3 Flux corrective transport

Another way to guarantee boundedness is flux corrective transport (FCT), first introduced by Boris and Book [18], and later generalised and extended to multi-dimensions by Zalesak, [19]. The boundedness is guaranteed by limiting the face flux in contrast to the face values of TVD/NVD schemes. But, FCT was found to be working well for analytical steady cases but non-mass conservative for practical cases [20].

OpenFOAM guarantees boundedness and stability to its solver with this flux corrective transport termed as multi-dimensionsal limiter for explicit solution (MULES), which is in lines with Zalesak et al. [19] implementation. The semi-implicit variant of MULES, first executes

| | |
|---|---|
| when $0 < \phi_i \leq k_1$ | $\phi_f^{CM} = \tilde{\phi}_i / Co_f$<br>$\gamma_f = \frac{\phi_f^{CM} - \tilde{\phi}_i}{1 - \tilde{\phi}_i}$ |
| when $k_1 < \phi_i \leq k_2$, | $\phi_f^{HC} = \tilde{\phi}_i / Co_f$<br>$\phi_f^{UQ} = [8 Co_f \phi_i + (1 - Co_f)(6\phi_i + 3)]/8$<br>$\phi_f^{CM} = \cos\theta \phi_f^{HC} + (1 - \cos\theta)\phi_f^{UQ}$<br>$\gamma_f = \frac{\phi_f^{CM} - \tilde{\phi}_i}{1 - \tilde{\phi}_i}$ |
| when $k_2 < \phi_i < k_3$, | $\phi_f^{UQ} = [8 Co_f \phi_i + (1 - Co_f)(6\phi_i + 3)]/8$<br>$\phi_f^{CM} = \cos\theta + (1 - \cos\theta)\phi_f^{UQ}$<br>$\gamma_f = \frac{\phi_f^{CM} - \tilde{\phi}_i}{1 - \tilde{\phi}_i}$ |
| when $k_3 \leq \phi_i \leq 1$, | $\gamma_f = 1$ (backward scheme) |
| else | $\gamma_f = 0$ (upwind scheme) |

Table 3: HC - Hyper-C scheme [16], UQ - ULTIMATE-QUICKEST scheme [16] and CM - CICSAM. Here, when face flux ($\mathbf{v}_f \cdot S_f > 0$), $\gamma_f = 1 - \gamma_f$ and vise versa.

an implicit predictor step, based on purely bounded numerical operators, e.g. Euler implicit in time, upwind for convection, etc., before constructing an explicit correction on which the MULES limiter is applied. All cases in this paper uses this MULES limiter.

## 3. RESULTS AND DISCUSSIONS

Air injected inside the cavity maintains an air layer. A wave is generated inside the cavity which reattaches at the beach plate, making a pressure force there. Fig. 3a shows the computational visualisation of the 3D wave surface hitting the beach plate. Fig. 3b shows the pressure contours with the velocity that illustrates the recirculation of air inside the cavity. Some of the air that leaks from the cavity is carried by the water along aft plate which reduces the wall shear stress and therefore the computed force.

Pressure induced force is the dominant contribution to the beach plate, whereas, force due wall shear stress is dominant in cavity and aft plate. The wall shear stress inside the air cavity is negligible due to small air velocity compared to that of water.

Table 4, shows the aft forces and cavity forces (cumulative forces from the cavity-roof and beach plate). Measurements from various numerical settings are compared and validated with experimental results. The forces computed is a summation of viscous (kinematic and turbulent) and pressure force.

With case A, case E and case J, all setting are identical except $\alpha$ convection scheme where it changes from Van Leer to SUPERBEE to CICSAM respectively. From case A to E to J, it can be seen, from Fig. 4, that the aft force gets closer to the experimental value but the beach force deviates. Same trend can be observed from case B to F to K, where the only change with respective to cases A, E and J is using linear scheme instead of limited linear scheme for counter-gradient $\alpha$ term. Moreover, the aft force is closer to experiments for case B with respect to case A but vice versa for beach force. Thus, when more compressive linear scheme is used, the aft force is predicted better, but under-predicts beach force. More compressive schemes distorts the wave profile formed inside the cavity which results in under-predicted beach force. Same is observed from case E to F and case J to K.

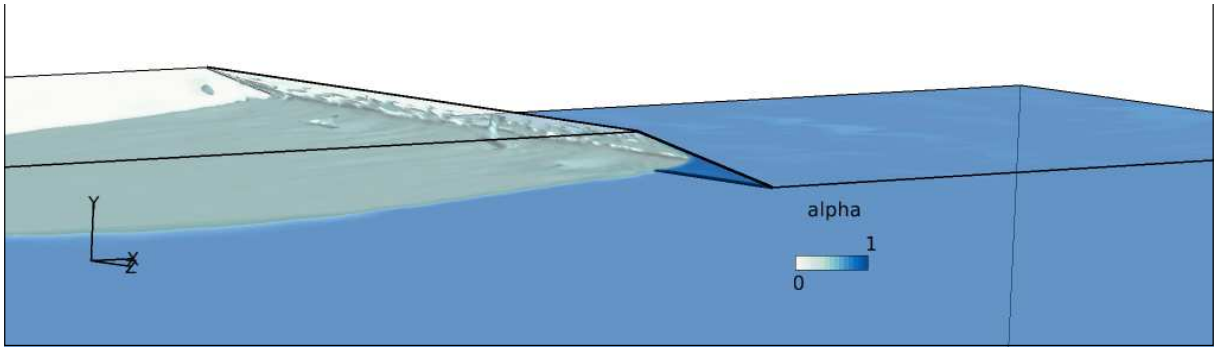


(a)

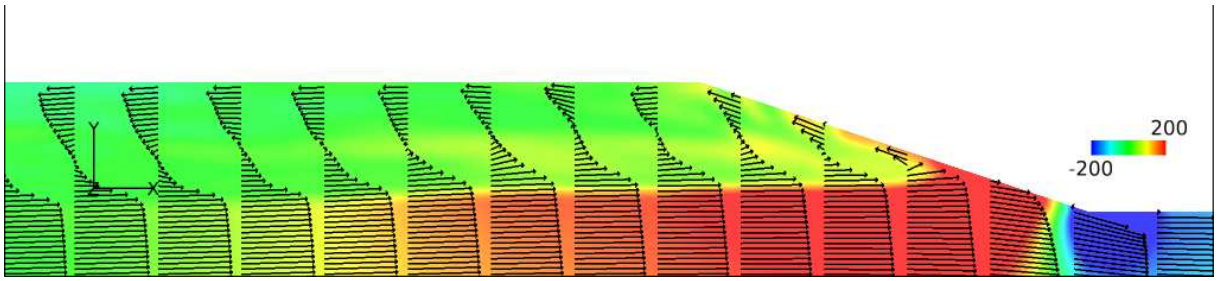


(b)

**Figure 3**: (a) Visualisation of the 3D wave surface hitting the beach plate, (b) Pressure ($p_{\rho gh} = p - \rho gh$) contour at the beach region of cavity. Velocity vectors are also shown.

| Case | $\partial \alpha v_j / \partial x_j$ | $\partial v_j^c \alpha(1-\alpha)/\partial x_j$ | $c\alpha$ | Aft (N) (Err.%) | Cavity (N) | Sum (N) (Err.%) |
|---|---|---|---|---|---|---|
| A | Van Leer | LL | 0.5 | 6.65 (32.96) | 13.20 | 19.85 (12.90) |
| B | Van Leer | linear | 0.5 | 7.20 (27.41) | 10.72 | 17.92 (21.36) |
| C | Van Leer | linear | 1 | 9.18 (07.45) | 10.61 | 19.79 (13.16) |
| D | Van Leer | IC | 1 | 9.20 (07.25) | 10.50 | 19.70 (13.55) |
| E | SUPERBEE | LL | 0.5 | 8.00 (19.35) | 12.60 | 20.60 (09.61) |
| F | SUPERBEE | linear | 0.5 | 8.20 (17.33) | 10.40 | 18.60 (18.38) |
| G | SUPERBEE | linear | 1 | 9.40 (05.24) | 09.75 | 19.15 (15.97) |
| H | SUPERBEE | linear | 2 | 8.70 (12.29) | 08.90 | 17.60 (22.77) |
| I | CICSAM | LL | 0 | 1.05 (84.87) | 18.02 | 19.07 (16.32) |
| J | CICSAM | LL | 0.5 | 9.61 (03.13) | 10.20 | 19.81 (13.07) |
| K | CICSAM | linear | 0.5 | 9.66 (02.62) | 09.71 | 19.37 (15.00) |
| L | CICSAM | IC | 0.5 | 9.58 (03.42) | 10.30 | 19.88 (12.77) |
| M | CICSAM | LL | 1 | 9.81 (01.10) | 09.30 | 19.11 (16.14) |
| N | CICSAM | LL | 2 | 9.05 (08.77) | 09.53 | 18.58 (18.47) |
| | Exp. [6] - | - | - | 9.92 | 12.87 | 22.79 |

Table 4: Comparative force measurement for different schemes. Here, IC is the interface-compression scheme. Limited linear scheme is used convective term ($\partial v_i v_j / \partial x_j$) for all cases except case C

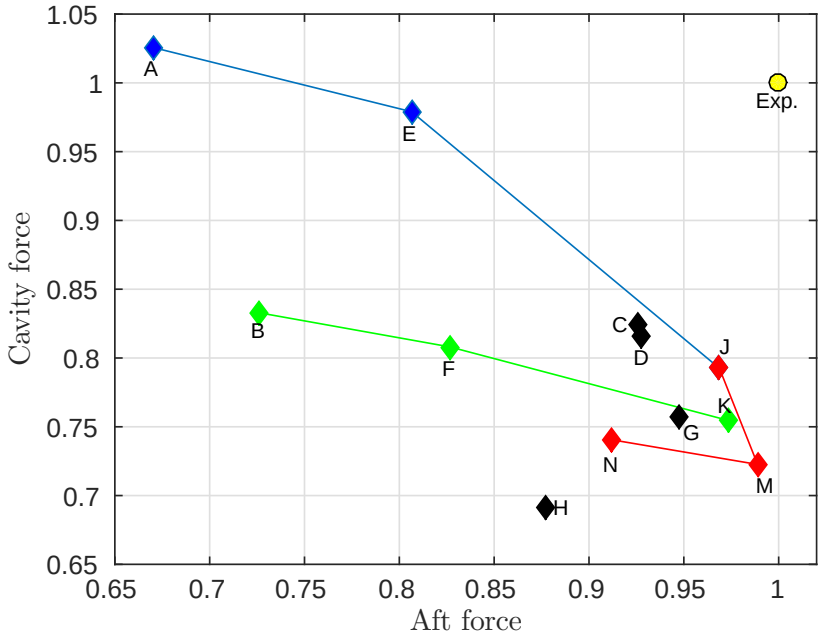


**Figure 4**: Forces for different cases from table 4, normalised with the experimental value.

When comparing cases F,G and H, forces are quite similar to each other, and thus it can concluded that scheme linear, limited linear and interface compression does not make a huge difference to wave capturing and multiphase wall shear stress.

For cases I, J, M and N, $c\alpha$ value (see Eq. 3), is increased while keeping other values identical. It can be seen from Fig. 4 that similar tread is followed for case J and M. But, when $c\alpha$ is increased to 2 (case N) from 1 (case M), aft force reduces and beach force increases, contradicting the expectation. This proves to conclude that over-compression with the nonphysical $c\alpha$ is undesirable after a certain value. Furthermore, Fig. 5 shows the wave profile for different value of $c\alpha$ with SUPERBEE and CICSAM schemes for convective $\alpha$ term. The wave profile matched well in the upstream of the cavity, but varies at the beach plate region.

## 4. CONCLUDING REMARK

The air cavity concept was studied computationally, with focus on the interface capturing between two phases, air and water. It was realised that, when more compressive techniques are used to better capture the interface in the boundary layer, it distorts the wave profile formed inside the cavity. Thus, a balance was required to capture both without compensating too much on the other. Moreover, finer meshes are required to nullify the effects of turbulence and schemes to better predict the results.

## 5. ACKNOWLEDGMENT

The project is funded by the Swedish Energy Agency, project 38284-1, Knowledge and methodology development for the analysis of air cavity ships. The computations were performed on resources at Chalmers Centre for Computational Science and Engineering (C3SE) provided by the Swedish National Infrastructure for Computing (SNIC).

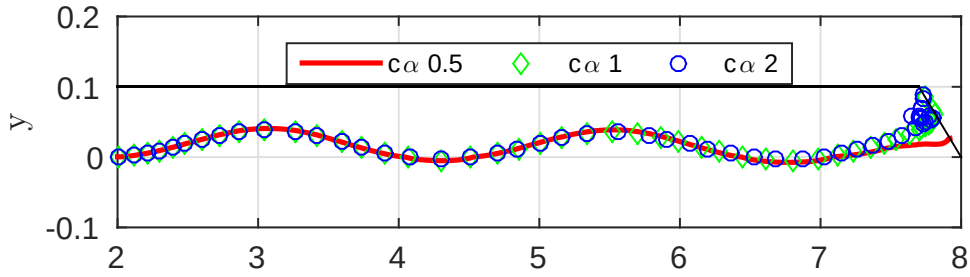


(a)

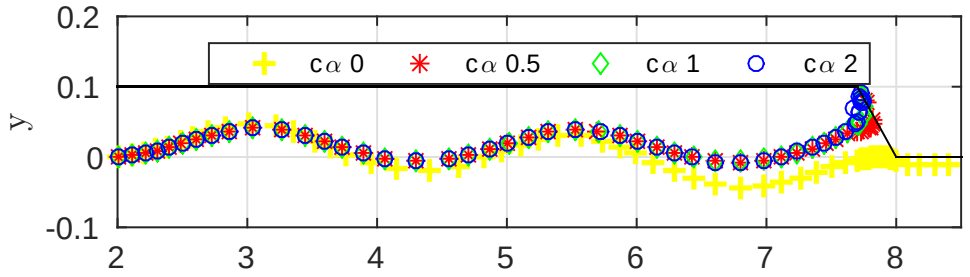


(b)

**Figure 5**: The wave profile inside the cavity is shown. Profiles are iso-surface of the VOF variable, α at 0.5; (a) three cases F, G and H (b) Four cases I, J, M and N; from Table 4

## 6. REFERENCES


1. Butuzov, A. A. (1967). Artificial cavitation flow behind a slender wedge on the lower surface of a horizontal wall. *Fluid Dynamics*, 2(2), 56-58.

2. Butuzov, A., Sverchkov, A., Poustoshny, A., and Chalov, S. (1999). State of art in investigations and development for the ship on the air cavities. *In International Workshop on Ship Hydrodynamics (IWSH99)*, China (pp. 1-14).

3. Latorre, R. (1997). Ship hull drag reduction using bottom air injection. *Ocean engineering*, 24(2), 161-175.

4. Matveev, K. I. (2003). On the limiting parameters of artificial cavitation. *Ocean Engineering*, 30(9), 1179-1190.

5. Matveev, K. I., Burnett, T. J., and Ockfen, A. E. (2009). Study of air-ventilated cavity under model hull on water surface. *Ocean Engineering*, 36(12), 930-940.

6. Abolfazl, S., Leer-Andersen, M., Bensow, R., and Norrby, J. (2012). Hydrodynamics of a Displacement Air Cavity Ship. *In 29th Symposium on Naval Hydrodynamics*, Gothenburg, Sweden

7. Hirt, C. W., and Nichols, B. D. (1981). Volume of fluid (VOF) method for the dynamics of free boundaries. *Journal of computational physics*, 39(1), 201-225.

8. Weller, H. G. (1993). The development of a new flame area combustion model using conditional averaging. *Thermo-fluids section report TF*, 9307.

9. WeHrvoje Jasak, Wikki Ltd.ller, H. G. (2008). A new approach to VOF-based interface capturing methods for incompressible and compressible flow. OpenCFD Ltd., Report TR/HGW/04.

10. Brackbill, J. U., Kothe, D. B., and Zemach, C. (1992). A continuum method for modeling surface tension. *Journal of computational physics*, 100(2), 335-354.

11. Issa, R. I. (1986). Solution of the implicitly discretised fluid flow equations by operator-splitting. *Journal of computational physics*, 62(1), 40-65.

12. Versteeg, H. K., and Malalasekera, W. (2007). An introduction to computational fluid dynamics: the finite volume method. *Pearson Education*.

13. Van Leer, B. (1974). Towards the ultimate conservative difference scheme. II. Monotonicity and conservation combined in a second-order scheme. *Journal of computational physics*, 14(4), 361-370.

14. Roe, P. L. (1985). Some contributions to the modelling of discontinuous flows. In *Large-scale computations in fluid mechanics* (pp. 163-193).

15. Hrvoje Jasak, Wikki Ltd. http://extend-project.de/

16. Ubbink, O. (1997). Numerical prediction of two fluid systems with sharp interfaces, Doctoral dissertation, University of London.

17. http://www.openfoam.org

18. Boris, J. P., and Book, D. L. (1973). Flux-corrected transport. I. SHASTA, A fluid transport algorithm that works. *Journal of computational physics*, 11(1), 38-69.

19. Zalesak, S. T. (1979). Fully multidimensional flux-corrected transport algorithms for fluids. *Journal of computational physics*, 31(3), 335-362.

20. Gopala, V. R., and van Wachem, B. G. (2008). Volume of fluid methods for immiscible-fluid and free-surface flows. *Chemical Engineering Journal*, 141(1), 204-221.